# Micellization and Gelation of Symmetric Triblock Copolymers with Insoluble End Blocks

**Mai Nguyen-Misra and Wayne L. Mattice***

*Institute of Polymer Science, The University of Akron, Akron, Ohio 44325-3909*

*Received July 25, 1994; Revised Manuscript Received December 9, 1994*®

ABSTRACT: In this work, the formation of micelle and gel from symmetric ABA triblock copolymers in selective solvents is followed using the Monte Carlo technique. The solvent is taken to be athermal for the middle block and poor for the end blocks. The effects of the block size and solubility of the end block A on system properties are explored with a focus on the critical micelle concentration (CMC) and critical gel concentration ($\phi_{gel}$*). The relevant micellar and/or network parameters, including the weight-average aggregation number, number density, and functionality, are obtained. Copolymer chain population distributions of the elastically active chains (bridges) and the elastically inactive chains (loops, free, and dangling chains) are calculated. Both the CMC and $\phi_{gel}$* are strongly dependent on the degree of incompatibility ($(2N_A)\beta\epsilon$, a variable which shows the combined effects of both the size and the solvent insolubility of the end block A) but only weakly dependent on the middle block size. As incompatibility increases, the CMC shows a slower decrease than the exponential decay predicted by Leibler et al. (*J. Chem. Phys.* **1983**, *79*, 3550) for diblock copolymers at high incompatibility. The dependence of the CMC and $\phi_{gel}$* on incompatibility appear to fit power-law type expressions, $y \sim x^{-a}$, where $y$ is either the CMC or $\phi_{gel}$* and $x$ is a scaling variable $(2N_A)\beta\epsilon$. The scaling exponent $a$ is approximately 0.4 for the CMC and is in the range 0.1−0.2 for $\phi_{gel}$*. The phase diagram appears complex, containing four regions, exhibiting homogenity, micellization, gel formation, and possible precipitation.

## Introduction

Association of block copolymers in a solvent which is poor for one block (block A) and good for the other block (block B) can produce structures like micelles and physical networks, which find potential applications ranging from controlled release to rheological modifications.[1-6] The phase behavior of ABA triblock copolymers is complex and is not well understood. On the other hand, the phase behavior of AB diblock copolymers in dilute solution has been well characterized, both theoretically[7-14] and experimentally.[15-20] The copolymer chains tend to associate, forming aggregates called micelles. The micelles consist of two main regions, an inner core containing the insoluble A blocks and an outer corona containing both the soluble B blocks and the solvent molecules. While both diblock and triblock copolymers can form micelles of similar shape, the polymer chains in the latter can adopt more topologies.

A diblock chain in a micelle can only be found in a dangling topology in which the A block is in the micellar core and the B block is dangling in the corona, whereas an ABA triblock chain can form a loop (both A blocks belong to the same micellar core), a bridge (each A block is in a different core), or a dangling chain similar to that of a diblock chain (Figure 1).[21] The ability of self-associated triblock chains to bridge two insoluble regions is one main feature distinguishing them from self-associated diblock chains.[22-24] This distinction leads to a very important qualitative difference in the phase behavior of the two systems; namely, that ABA triblock chains can form a networked structure. This qualitative difference also leads to different viscoelastic behavior for the two systems. At low concentrations solutions of diblock copolymers behave like fluid suspensions of soft particles. The viscoelastic behavior exhibited by diblock copolymers, at high concentrations, is dominated by extensive entanglements of the B blocks in the corona of the close-packed micelles, referred to as a macrolattice

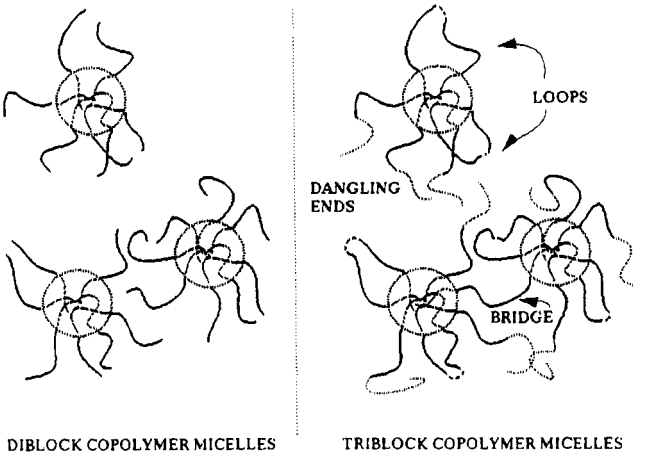


**Figure 1.** Possible micellar chain topologies for diblock (dangling end) and ABA triblock (dangling end, bridge and loop) copolymer chains in selective solvents.

structure.[25-29] This structure has also been observed for the equivalent system of BAB triblock copolymers.[30-34] In an ABA triblock system, on the other hand, gelation could occur by bridging of the micelles in addition to entanglements[35] at high concentrations. Due to the differences in the mechanisms of "gel formation" for a diblock and a triblock system, their viscoelastic behavior is also different. Not only would a triblock copolymer gel have a higher elastic modulus but also a larger average lifetime (broader rubbery plateau region). Furthermore, at zero or very low shear strain rate, a diblock "gel" would behave like a fluid because of gradual disentanglements whereas an ABA triblock gel would have a finite elastic response.[36]

Although there are several contrasting features between the association behavior of the two systems, the driving force for association is the same, the reduction of the enthalpic contribution, at least for nonaqueous systems.[7-14] At very low polymer concentrations, chains remain free in order to maximize their translational entropy. As the concentration is increased, one reaches

® Abstract published in *Advance ACS Abstracts,* February 1, 1995.

0024-9297/95/2228-1444$09.00/0 

a critical concentration (CMC) where it is favorable for the insoluble blocks to associate and trade their translational freedom in order to reduce their enthalpy. The CMC is strongly dependent on the degree of incompatibility, $\chi N_A$.[8,37] Here, $N_A$ is the length of the insoluble block and $\chi$ is the quasibinary Flory–Huggins interaction parameter. For the long chain diblock copolymers ($N_A \gg 1$) in selective solvents, it is well established that micellization occurs at relatively low concentrations and low values of $\chi$.[15–20] Experimental evidence indicates that at concentrations close to the CMC, the micelles are spherical in shape; the block asymmetry determines the micellar geometry. At higher concentrations the number density of micelles increases, and eventually entanglements between dangling blocks of the close-packed micelles leads to "gel" formation.[25–27]

In contrast, the phase behavior of ABA triblock chains in dilute solution is not as well characterized, although several recent works have looked at self-association of symmetric triblock copolymers in melts leading to lamellar mesophases, by scaling and self-consistent mean field arguments.[22–24]1,[38–40] The results of the existing studies, both theoretical[21,41] and experimental[15,16,19,42–44] on ABA triblock systems are sometimes at odds with each other; basic issues such as the occurrence of micelles or networked structures remain unresolved. Below we examine some of the salient experimental and theoretical results from previous studies on self-association of triblock copolymers.

The experimental results of Tanaka and co-workers[16] and Tang et al.,[43] lead to the conclusion that micellization of ABA triblock chains is improbable. Tanaka et al., using viscometry and sedimentation, did not observe micellization for poly(methyl methacrylate)–polystyrene–poly(methyl methacrylate) in mixed solvents of toluene (common solvent) and *p*-cymene (good middle block solvent). The results of Tang et al., on poly(2-vinylpyridine)–polystyrene–poly(2-vinylpyridine) in toluene, a good solvent for polystyrene, appeared to confirm the conclusion of Tanaka et al., that micellization does not occur.

The early work by Krause,[42] on the other hand, was the first to report evidence of micellization in triblock copolymers. Using light scattering Krause observed micellization for poly(methyl methacrylate)–polystyrene–poly(methyl methacrylate) in either acetone, a poor solvent for polystyrene, or triethylbenzene, a good solvent for polystyrene. Micellization was also observed by Balsara et al.[21] for poly(2-vinylpyridine)–polystyrene–poly(2-vinylpyridine) in toluene using dynamic light scattering. They, however, did not observe any branched, or network-like structure. A recent work by Zhou and Chu on poly(oxypropylene)–poly(oxyethylene)–poly(oxypropylene) in water, which is a poor solvent for poly(oxypropylene), shows convincingly that micellization for this system can occur, at least over a limited range of concentration and temperature.[44] In another study, using light scattering, Tanaka and co-workers[19] observed micellization and an aggregate resembling a network-like structure for a system of poly(methyl methacrylate)–polystyrene–poly(methyl methacrylate).

A somewhat contradictory picture also emerges on the theoretical side. ten Brinke and Hadziioannou[41] and Balsara et al.[21] attempted to explain their experimental results using simple mean field models. The most important feature in a mean field model is the assumption of constant segment density, in both the micellar core and the corona. Most of the assumptions were similar for the two models except for the expressions for the entropic loss due to loop formation in triblock copolymers.

Looking at the back-folding of loops in terms of a chain cyclization process, ten Brinke and Hadziioannou estimated the free energy associated with entropic loss for back-folding of the middle block, $F_{loop}$. A factor, $\beta_L$ ($\sim O(1)$), was introduced to correct for the difference between macrocyclization of a homopolymer corresponding to the middle block and the back-folding of the triblock copolymer. Their results showed the existence of a critical value of $\beta_L$, typically below 1 for most conditions, above which micelles could not exist. Since for polymers $\beta_L \geq 1$, they concluded that micellization was impossible, thereby supporting their experimental observations. Balsara et al.[21] suggested that ten Brinke and Hadziioannou may have overestimated the penalty for loop formation. To estimate $F_{loop}$, they derived an expression for the conformational entropy of a Gaussian chain with both ends confined in the shell of thickness $\Delta$, where $\Delta$ is the thickness of the core–corona interface. By incorporating this expression for $F_{loop}$, in the total free energy calculation, Balsara et al. found that micellization is indeed possible. Both models,[21,41] however, excluded the dangling and bridging structures. This is a major drawback since it restricts their analysis to low concentrations and high incompatibility. In a recent study, Linse[45] investigated the effects of chain architecture on the aggregation behavior using a Scheutjens and Fleer-type lattice approach. They found that ABA triblock copolymer chains do form micelles although only at high concentrations and a narrow temperature range, as compared to diblock copolymer and BAB triblock copolymer systems.

Our motivation for carrying out this study is in part due to the lack of a comprehensive understanding of the phase behavior of ABA triblock copolymers in solution and also because of the results from a recent Monte Carlo study from our group,[46] which showed that micellization is possible under certain conditions. In order to make the analysis tractable, the existing theoretical models have to invoke many assumptions. In this study, we follow a system of ABA triblock copolymers in solvents that are selectively poor for the end blocks and athermal for the middle block using an on-lattice Monte Carlo model. One major advantage of using a simulation technique is that very few major assumptions are necessary.

We are interested in determining the conditions under which micellization could occur, specifically in terms of the dependence of CMC on incompatibility and middle block size. The ability of this system to form a 3-D thermoreversible network, which has not been looked at before, is also explored in terms of the dependence of the critical sol-to-gel transition on incompatibility and middle block size. The critical sol-to-gel transition results could be readily verified experimentally via oscillary shear viscosity measurements. For this study, only thermodynamic properties of the triblock network are calculated and discussed. The geometric properties will be presented elsewhere. The relevant equilibrium properties, including the population density of the four states (free, loop, bridge, and dangling end), micelle and cluster average aggregation numbers, micelle number density, and network functionality, are presented. The instantaneous relaxation modulus, $G_g$, is also calculated for the purpose of comparison. Experimentally, these parameters could be measured using static and dynamic

light scattering, pulsed field gradient NMR, fluorescence, and dynamic mechanical measurements.

This manuscript is organized into four main sections. Following the Introduction, the on-lattice Monte Carlo model used in this study will be described in detail in section 2. In section 3, the relevant results associated with the micellization, gelation, and precipitation behavior will be presented and discussed. There, it will be shown that the finite box size effects on the association behavior are not significant at the selected box size. The conclusions from this study will be summarized, via the phase diagram, in the last section.

## Model

The discussion of our model is broken down into two sections. In the first part, we will discuss the main system variables, including, $L$, $N_A$, $N_B$, and the interaction energy parameter. The Monte Carlo technique will be described in the second section.

**System Variables.** The system in this study was simulated using an on-lattice Monte Carlo technique. Cubic lattices of size $L \times L \times L$ with periodic boundary conditions in all three directions $x$, $y$, and $z$ were employed. To minimize any possibility of size effects, we chose a box size of 40 so that it is much larger than the dimensionless *root-mean-square* end-to-end distance, $\langle r^2\rangle^{1/2}$. The range of chain lengths employed was from $N = 30$ to 70 corresponding to a change in $\langle r^2\rangle^{1/2}$ from ~8 to 13. Since the box size used in this study was more than three times $\langle r^2\rangle^{1/2}$, it is unlikely that there would be any size effects insofar as the behavior of single chains is concerned.

We are primarily interested in the system when there is cooperative behavior of the chains. At $\phi \sim$ CMC ($\phi = 0.02$) and $N = 70$, the longest chain length considered in this study, the independent micelles in our simulations have a maximum diameter of approximately 14 lattice units, which is not much larger than for the single chain and typically no larger than one-third of $L$, the box size. (The micelle radii of gyration were calculated by averaging over micelles of the same aggregation number for the last 50 system moves. The diameter reported above corresponds to the largest micelle in the system under those conditions.) It is therefore unlikely for an independent micelle to interact with its images in the neighboring cells.

The micelles clearly do interact (directly or indirectly) with their periodic images when they form a three-dimensional network. The hypothesis that the gel point, $\phi_{gel}^*$, evaluated in our simulations at finite $L$ can be related approximately to the limiting behavior, $\phi_{gel,\infty}^* = \lim \phi_{gel,L}^*$, rests on the assumptions that the transition from the sol state to the gel state is highly cooperative and that our simulations are for systems large enough to capture the cooperative unit. To study the size effects, $L$ was varied from 30 to 50 keeping other variables constant ($N_A = 15$, $N_B = 10$, and $\beta\epsilon = 1$). A more detailed analysis is presented in the next section.

In this study, the triblock copolymers under investigation were symmetric, e.g., $A_{N_A}B_{N_B}A_{N_A}$. The interaction energy between i and j was assumed to be nonzero and positive if i = A and j = B or S, $\Delta\epsilon_{AB} = \Delta\epsilon_{AS} = \epsilon > 0$, and zero otherwise. This situation would be realized when the interaction energy between like molecules was small enough to be neglected (or taken as background) and the solvent molecules and the B block possessed similar properties. This quasibinary interaction energy is related to the Flory–Huggins interaction energy parameter, $\chi_{FH}$,

$$\chi_{FH} = \frac{\Delta\epsilon_{AS} z}{k_B T} \tag{1}$$

where $z$ is the lattice constant.

**Table 1. System Variables**

Incompatibility Effects, $L = 40$, $N_B = 10$

| $2\beta\epsilon N_A$ | $N_A$ | $\beta\epsilon$ | $\phi$ |
|---|---|---|---|
| 2 | 10 | 0.1 | 0.084–0.11 |
| 3 | 15 | 0.1 | 0.010–0.11 |
| 4 | 20 | 0.1 | 0.075–0.11 |
| 5 | 25 | 0.1 | 0.020–0.094 |
| 9 | 15 | 0.3 | 0.010–0.11 |
| 15 | 15 | 0.5 | 0.010–0.13 |
| 20 | 10 | 1.0 | 0.020, 0.056 |
| 30 | 15 | 1.0 | 0.010–0.14 |
| 40 | 20 | 1.0 | 0.020–0.094 |
| 50 | 25 | 1.0 | 0.020, 0.047, 0.056 |
| 60 | 15 | 2.0 | 0.010–0.10 |
| 90 | 15 | 3.0 | 0.010–0.10 |

Middle Block Size Effects, $L = 40$, $N_A = 15$, $\beta\epsilon = 1.0$

| $N_B$ | $\phi$ |
|---|---|
| 10 | 0.010–0.14 |
| 15 | 0.020–0.084 |
| 20 | 0.010–0.11 |
| 30 | 0.010–0.11 |
| 40 | 0.020–0.084 |

Lattice Size Effects, $N_A = 15$, $N_B = 10$, $\beta\epsilon = 1.0$

| $L$ | $\phi$ |
|---|---|
| 30 | 0.046–0.11 |
| 40 | 0.010–0.14 |
| 45 | 0.040–0.08 |
| 50 | 0.037–0.08 |

To characterize the incompatibility effects, $N_B$ was kept constant at 10. The degree of incompatibility, $2N_A\beta\epsilon$, was varied from 2 to 90, where $\beta = (k_B T)^{-1}$. This was accomplished by using combinations of different $N_A$ and $\beta\epsilon$ with $N_A = 10$, 15, 20, or 25 and $\beta\epsilon$ ranging from 0.1 to 3.0. In Table 1, the system variables studied are listed. This range of incompatibility was chosen to cover both the weak and strong segregation limits. Experimentally, this could be accomplished by changing the temperature or varying the solvent ratio if a mixed solvent system is used.

The effects of the middle block size in the strong segregation regime ($\beta\epsilon = 1$) were investigated. In this part of the study, the size of the end block $N_A$ was maintained at 15. $N_B$ was varied from 10 to 40.

For each set of values $\{N_A, N_B, \beta\epsilon\}$, the concentration was varied. The concentration range studied, $\phi < 0.15$, fell in the dilute range $\phi < \phi^*$, where $\phi^*$ is the overlap concentration $\sim N/(4/3\pi R_g^3)$. The overlap concentration was calculated to be approximately 0.20 for a chain length of 40 (using $\beta\epsilon = 0$).

**Simulation Details.** Initial conformations were generated by randomly placing the chains on the lattice, satisfying the conditions of self-avoidance and mutual avoidance. The chains were allowed to relax under zero interaction energy, satisfying only the requirements of excluded volume. The types of moves used were the typical Monte Carlo moves including reptation, kink-jump, and crankshaft.[47] First, the chain to be moved was picked randomly and the chain end to be reptated was also chosen randomly. Reptation was allowed if the self-avoidance and mutual avoidance conditions were not violated. Subsequently, a segment on that chain

was randomly chosen. If the chosen segment was an end segment, then again reptation was attempted. If it was an internal segment, then it was either kink-jumped or crankshafted, if either was allowed. Ten million moves were attempted in order to generate the initial disordered state. The energy was then "turned on". The system was allowed to equilibrate under the self-avoidance, mutual avoidance, and Metropolis conditions. Simply stated, the Metropolis condition specified the probability of an attempted move as

$$P = \min\left\{1, \exp\left(\frac{\Delta E}{k_B T}\right)\right\} \tag{2}$$

If a move was not allowed, the old configuration still was counted as the new state. Typically, the system reached dynamic equilibrium after 5 million attempted moves. To determine if there was any hysteresis in the properties, simulations of the same system ($N_A = 15$, $N_B = 10$, $\phi = 0.075$ or 0.094) were performed with increasing interaction energy (forward step) and then decreasing energy along the same path (reverse step). The change in interaction energy $\epsilon$ was in an increment of 1 $k_BT$. The final state of a simulation was used as the initial state of the next higher (forward step) or lower (reverse step) energy simulation. The lack of hysteresis in our results shows that this system is truly reversible.

The relevant micellar properties were calculated for the last 50 system moves (1 system move = $NM$ moves, where $N$ is the chain length and $M$ is the number of chains). These properties were averaged, and the corresponding standard deviations were calculated. The equilibrium properties calculated and presented in this paper were the population density of the four possible topologies (free, bridge, loop, and dangling), the average aggregation number of the micelles and the clusters, the cluster average functionality, and the micellar number density. Using the above quantities, both CMC and the sol → gel transition point were determined.

## Results and Discussion

The discussion of results is divided into two main sections. In the first section, the discussion is focused mainly on micellar properties such as the micellar aggregation number, $p$, the micelle number density, $n$, and chain population densities. Macrophase separation is also discussed briefly in this section. The second section is devoted to the discussion on gelation and the corresponding relevant parameters. Each section is further broken down into two subsections, with the first subsection dealing with the effects of the incompatibility, $2N_A\beta\epsilon$,[37] and the second with the effects of the middle block size, $N_B$. In this section, it will also be shown that there are minimal lattice size effects under the conditions investigated.

**I. Micellization and Chain Population Density.** In this study, a micelle is defined as a group of two or more chains having A−A interchain contacts. A cluster (of size $s$) is defined as a group of ($s$) interconnecting, or bridging, micelles. Hence, single micelles are considered as clusters of size $s = 1$. The micelle aggregation number $p$ is the weight-average quantity reported in terms of the number of A (end) blocks in the core of the micelle. The cluster aggregation number $w$ is presented as the number of copolymer chains. The weight-average aggregation numbers, $p$ and $w$, are given by eqs 3a and 3b, respectively, where $p_i$ and $w_j$ are the number of A blocks in micelle $i$ and the number of chains in cluster $j$, respectively, and $n$ and $q$ are the total number of micelles and the total number of clusters, respectively, in the system. The upper limit for both $n$ and $q$ is $\sim M/2$, or $\phi L^3/(2N)$ where $M$ is the number of copolymer chains in the system and $N$ is the total chain length, $2N_A + N_B$. Since the micelles in the clusters with $s > 1$ act as physical cross-links, $n$ can also be looked at as the cross-link density, in a unit volume of $L^3$. A bridge is a chain having each of its two insoluble end blocks anchored in different micellar cores. When both of its end blocks are in the same micelle, a chain is considered a loop. When only one of its end blocks is in a micelle and the other is dangling in solution, it is called a dangling chain. The above micellar variables may be related by the system variables, $\phi$ (the copolymer volume fraction), $L$ (the box dimension), and $N$ (the total chain length),

$$p = \frac{\sum_{i=1}^{n} p_i^2}{\sum_{i=1}^{n} p_i} \qquad w = \frac{\sum_{j=1}^{q} w_j^2}{\sum_{j=1}^{q} w_j} \tag{3a, b}$$

$$\sum_{i=1}^{n} p_i = p_n n = \frac{\phi L^3}{N}(2f_l + 2f_b + f_d) \tag{4}$$

where $p_n$ is the number-average micelle aggregation number, and $f_l$, $f_b$, and $f_d$ are the loop, bridge, and dangling fraction, respectively.[48] The sum of $f_l$, $f_b$, and $f_d$ is the fraction of chains in the micelles, $\xi$.

**A. Effects of Incompatibility and Concentration. Micellization and the CMC.** The incompatibility effects were characterized by using various combinations of $N_A$ and $\beta\epsilon$ (see Table 1). Grouping ($N_A$, $\epsilon$) into the parameter $x = 2N_A\beta\epsilon$ produces a master curve $F = F(x)$, where $F$ is a thermodynamic property. Figure 2 and the inset in this figure, respectively, depict the effects of concentration and incompatibility, $2N_A\beta\epsilon$, on micellization. Micellization is shown in the above plots as the fraction of chains in the micellar phase, $\xi$. Figure 2 shows micellization at selected incompatibility $2N_A\beta\epsilon = 3$, 5, 30, and 50 using various combinations of $N_A$ and $\beta\epsilon$ (see Table 1). Some representative error bars are included in this figure and subsequent figures in the manuscript. However, most uncertainties are smaller than the size of the symbols; those are not shown. As expected, $\xi$ is a strong function on both concentration and incompatibility, approaching 1 at higher values of interaction or concentration. $\xi$ increases monotonically with concentration, a behavior that is similar to that exhibited by diblock copolymers in solutions.[8] At low concentrations, when the enthalpic penalty is not severe, a large fraction of the copolymers remains free, resulting in a small fraction of chains in the micellar phase. As concentration increases, however, the number of unfavorable contacts increases. The increase in enthalpic interactions leads to increasing association of copolymers, at the expense of the loss in entropy. Similarly, micellization also increases as incompatibility or enthalpic penalty, increases (Figure 2 inset).

Micellization is shown in another form in Figure 3a, which is a plot of the CMC versus $2N_A\beta\epsilon$. The inset of Figure 3a illustrates how the CMC was estimated. In this study, the CMC is defined as the concentration below which there is no micelle. The CMC and the

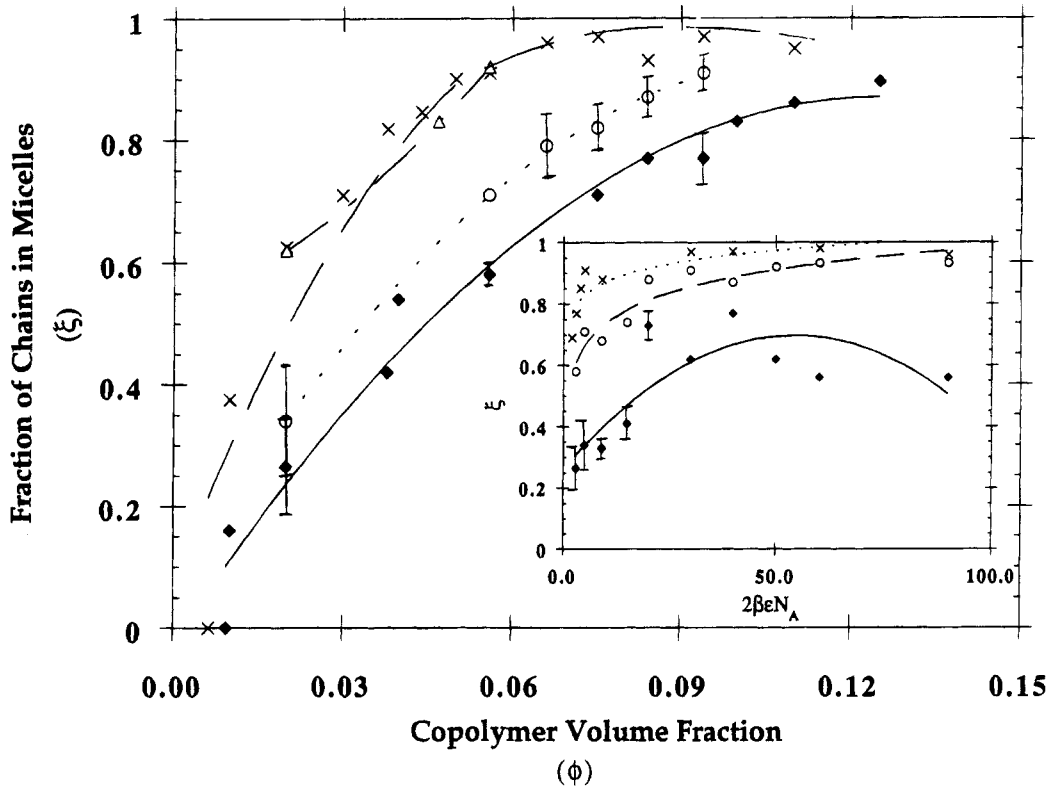


**Figure 2.** Dependence of $\xi$ on $\phi$ with $2\beta\epsilon N_A$ of (♦) 3, (○) 5, (×) 30, and (△) 50. In this figure and those that follow, unless indicated otherwise, the lines are drawn for visual guide. The inset shows the data in a different form, $\xi$ versus $2\beta\epsilon N_A$, with $\phi$ = 0.02 (♦, solid curve), 0.056 (○, dashed curve), and 0.094 (×, dotted curve).

corresponding errors were estimated by performing linear regression on the region above the CMC. In Figure 3, we see that the CMC decreases strongly as incompatibility increases in the low incompatibility range (weak segregation limit) but becomes saturated at very high incompatibility (strong segregation limit). Due to the stronger entropic effects associated with triblock copolymers, the dependence is weaker than the exponential dependence predicted for diblock copolymers in the strongly incompatible regime where the enthalpic effects dominate.[8,9] In fact, the CMC appears to have a power-law dependence on incompatibility.

$$\text{CMC} \sim x^{-b} \tag{5}$$

where $x$ is a scaling variable ($2N_A\beta\epsilon$) and $b \sim 0.4$. The effects of $L$ on the CMC was determined for $L$ ranging from 30 to 50 while $N_A$, $N_B$, and $\beta\epsilon$ were kept constant at 15, 10, and 1.0, respectively. Our results, included as Figure 3b, show that there is no systematic dependence of the CMC on the lattice size $L$, for the box size range investigated in this study.

**Micelle Aggregation Number and Number Density.** Parts a and b of Figure 4 show the effects of concentration on $p$ and $n$, respectively. For clarity, only a few representative results at selected incompatibilities are shown. Figure 4a shows that $p$ is relatively insensitive to concentration at low concentration for all levels of incompatibility. In weak segregation ($2N_A\beta\epsilon < 5$), $p$ remains relatively constant with concentration even at high concentrations. Once micellization has started, any newly added copolymers in the low-concentration range preferentially form new micelles, increasing $n$, rather than associate with the existing micelles. At low incompatibility ($2\beta\epsilon N_A = 2$ and 3 in Figure 4a,b), this trend remains even in the high-concentration regime. At higher incompatibility ($2\beta\epsilon N_A > 4$), however, our data show that above certain concentrations the micelles drastically increase in size while $n$ remains constant or increases only slightly. This onset of micellar growth or coalescence, which may eventually lead to precipitation (or macrophase separation) has been observed experimentally by Kotaka and co-workers.[15,16]

This observation of sudden micellar growth, which has not been seen in diblock copolymer systems, cannot be attributed to any change in the micellar geometry since it is observed that in general the micelles remain wormlike or cylindrical in shape. Furthermore, the increase in micellar size is restricted to only a few micelles. The micellar aggregation number becomes more polydisperse as either concentration or incompatibility increases. This observation seems to indicate some sort of coalescence of a group of two or more micelles. The bridging nature of the triblock copolymer chains which allows gel formation also leads to instability in the micelles (e.g., increase in micellar attraction). Further micellar growth may eventually lead to precipitation of the copolymers from solution. We denote the critical concentration where there is a change in slopes in $p$ versus concentration as the onset of precipitation, $\phi_M^*$. $\phi_M^*$ is located at the point of intersection of the two lines formed below and above $\phi_M^*$, respectively, in the plot of $p$ versus concentration.

In the insets of Figure 4a,b, the incompatibility effects are illustrated for three concentrations. In the low-concentration range, both $n$ and $p$ are seen to have weak dependence on incompatibility. In the high-concentration range the increase in $p$ with $2N_A\beta\epsilon$ is accompanied by a corresponding decrease in $n$ with $2N_A\beta\epsilon$ and vice versa; this is expected since $p$ and $n$ are inversely related to maintain constant $\xi$ at these concentrations. The appearance of a maximum in the $p$ versus $2N_A\beta\epsilon$ plot (or the corresponding minimum in the $n$ versus

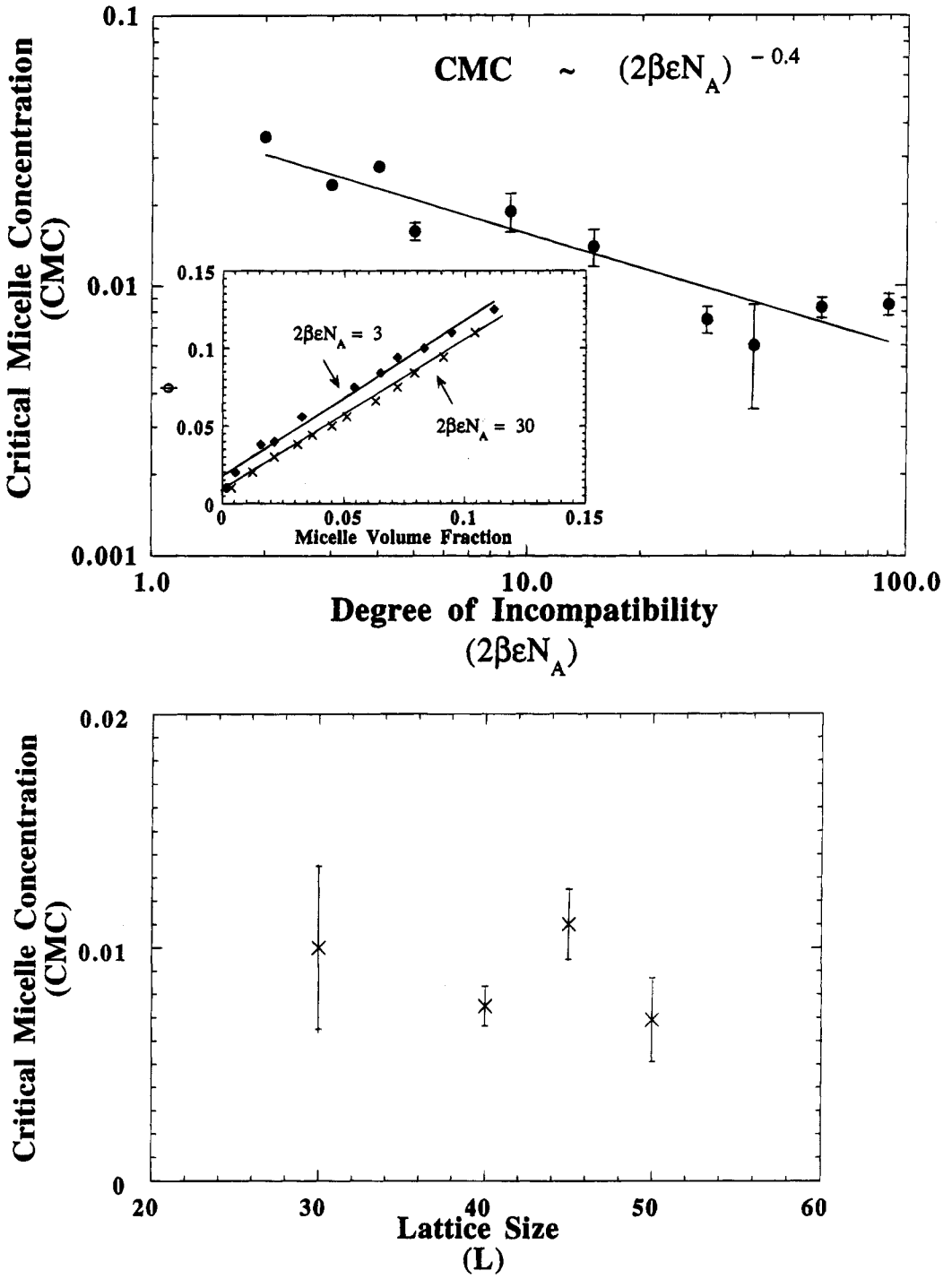


**Figure 3.** (a, top) Dependence of the CMC on $2\beta\epsilon N_A$. The solid line represents a power-law expression discussed in the text. The inset illustrates how the CMC is determined for a system of triblock copolymer chains of $N_A = 15$ and $N_B = 10$ with $2\beta\epsilon N_A$ of 3 (top line) and 30 (bottom line). (b, bottom) Dependence of the CMC on $L$ for a system of triblock copolymer chains of $N_A = 15$ and $N_B = 10$ with $\beta\epsilon = 1.0$.

$2N_A\beta\epsilon$ plot) at high concentrations suggests that micellar growth is most pronounced in the intermediate incompatibility range. In the strong segregation regime, both $n$ and $p$ are relatively independent of $2N_A\beta\epsilon$.

**Chain Population Density.** In Figure 5a–c, the variations with concentration of the dangling, loop, and bridging fractions are shown. The curves in each panel represent the results obtained at $2N_A\beta\epsilon$ of 3, 4, 9, 30, 40, and 90. The free chain fraction, $f_f = 1 - \xi$, decreases with concentration, as expected.

In the low-concentration range, the only possible topologies for a micellar chain are loop and dangling end. The bridging topology is not accessible due to a relatively large entropic penalty from stretching (at low concentrations, there are few micelles so the average intermicellar distance is large. Thus a bridging copolymer chain would be highly extended.) Therefore, loops and dangling ends compete in the low-concentration range. This competition depends on the degree of incompatibility. At low incompatibility, the dangling topology competes more favorably with the loop configuration, as reflected in Figure 5a,b, which show the dangling fraction, $f_d$, and the loop fraction, $f_l$, versus concentration, respectively. At low incompatibility ($2N_A\beta\epsilon < 10$), when the enthalpic interactions are small, $f_d$ increases faster with concentration and is larger in

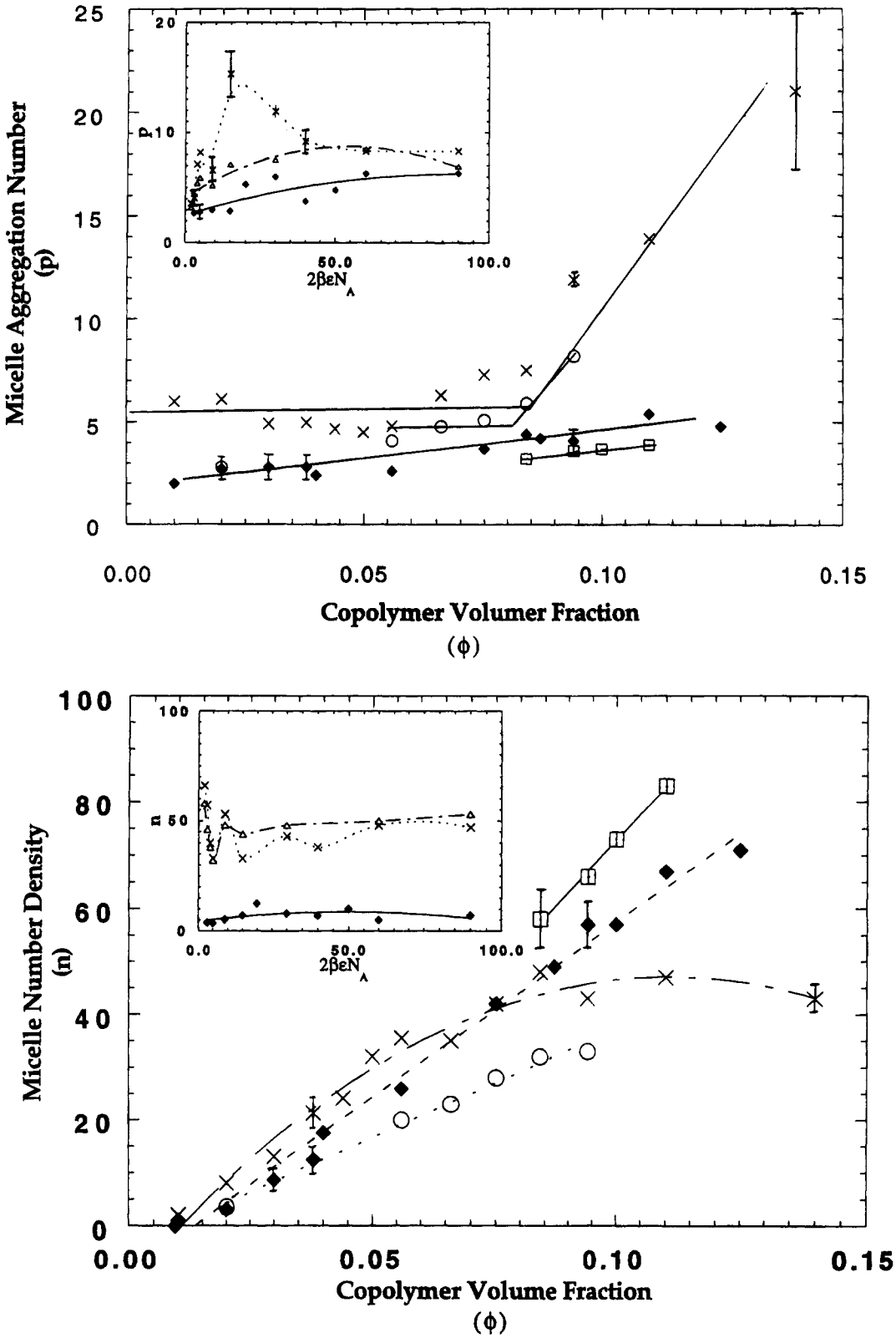


**Figure 4.** (a, top) Dependence of $p$ on $\phi$ with $2\beta\epsilon N_A$ of (□) 2, (♦) 3, (○) 5, and (×) 30. The inset shows the same data in a different form, $p$ versus $2\beta\epsilon N_A$ with $\phi$ of (♦, solid curve) 0.02, (△, dashed/dotted curve) 0.084, and (×, dotted curve) 0.094. (b, bottom) Variations of $n$ with $\phi$ with $2\beta\epsilon N_A$ of (□) 2, (♦) 3, (○) 5, and (×) 30. The inset shows $n$ versus $2\beta\epsilon N_A$ with $\phi$ of (♦, solid curve) 0.02, (△, dashed/dotted curve) 0.084, and (×, dotted curve) 0.094.

magnitude than $f_l$. At higher incompatibility ($2N_A\beta\epsilon \geq 30$), the reverse is true. The bridging fraction, $f_b$, increases with both concentration and incompatibility. Particularly, there appears to be a critical concentration below which $f_b$ is zero. This threshold appears to shift to lower concentration as incompatibility increases.

At higher concentrations, not only are there more micelles but the number of unfavorable contacts, or enthalpic interactions, in the system also increases. This environment is favorable for a bridging chain, since the average micellar distance becomes smaller, allowing bridging without significant chain stretching, but un-

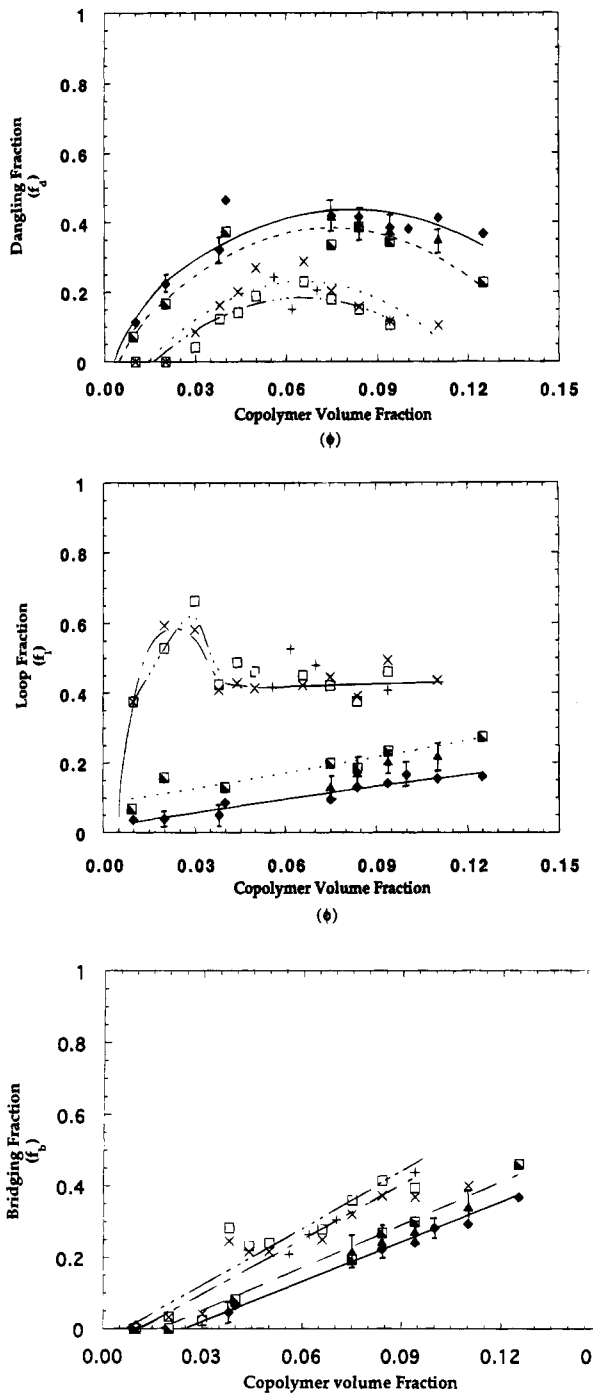


**Figure 5.** Fraction of (a, top) dangling ends, (b, middle) loops and (c, bottom) bridges versus $\phi$, for $2\beta\epsilon N_A$ of (♦) 3, (△) 4, (◪) 9, (×) 30, (+) 40, and (□) 90.

favorable for a dangling configuration, particularly at high incompatibility. In other words, the entropic terms become less significant as compared to the enthalpic terms. Thus in the high-concentration range, loops and bridges compete. Energetically, the major difference between a loop and a bridging topology is the stretching penalty associated with the bridging chain. The extent of this stretching penalty determines the relative population distribution. At low incompatibility, since the enthalpic contribution is small even in the high concentration range, $f_d$ remains constant at a high value. At higher degrees of incompatibility, $f_d$ decreases. Parts b and c of Figure 5 show that $f_l$ remains at a constant value, whereas $f_b$ continues to rise, as concentration increases.

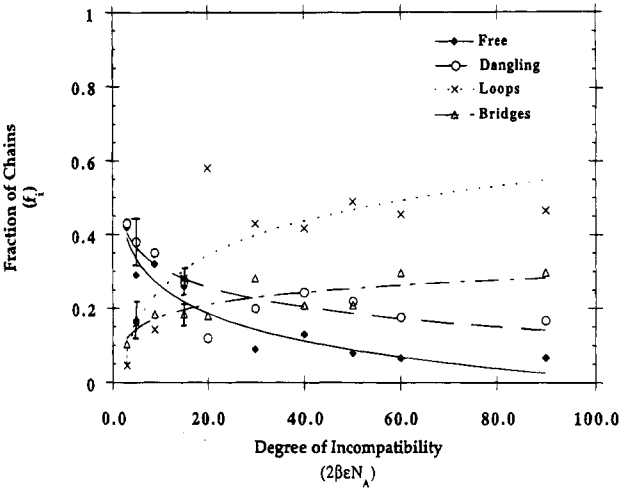


**Figure 6.** Variations of fraction of copolymer chains present as (♦, solid curve) free chains, (○, dashed curve) dangling ends, (×, dotted curve) loops, and (△, dashed/dotted curve) bridges with $2\beta\epsilon N_A$ at $\phi = 0.056$.

Figure 6 shows the effects of incompatibility on the free, loop, dangling, and bridging fractions at $\phi = 0.056$. This figure indicates that above a certain level of incompatibility, the chain populations become insensitive to the increase in incompatibility. The trends are similar at all concentrations, although the absolute magnitudes differ. At any fixed concentration, both $f_f$ and $f_d$ decrease while $f_l$ increases as incompatibility increases, due to the increase in enthalpic penalty. The bridging fraction increases very slightly with incompatibility at low concentration but becomes stronger at higher concentrations. As expected, $f_b$ is negligible as compared to $f_d$ or $f_l$ at low concentration, becoming significant only at higher concentrations. Again, in the low-concentration range, loops compete favorably with dangling chains. In the high-concentration range, the competition is between bridges and loops.

**B. Effects of the Middle Block Size, $N_B$. Micellization and the CMC.** Contrary to the existing belief,[21,41,44] our results indicate that $N_B$ does not affect the overall micellization behavior significantly. Figure 7, which is a plot of micellization, $\xi$, versus concentration for systems with triblock copolymer chains with varying middle block size $N_B$, indicates the relatively independence of micellization from $N_B$. This evidence is supported by the inset in Figure 7 which shows the CMC as a function of $N_B$. Although there is a slight increase in the CMC as $N_B$ increases from 10 to ~20 and a decrease in the CMC as $N_B$ increases from 20 to 40, these variations are relatively small. As we will see later, although $N_B$ does not affect the overall micellization behavior significantly, it does affect the chain distribution functions.

**Micelle Aggregation Number and Number Density.** Figure 8 and its inset show $p$ and $n$ as a function of the middle block size, $N_B$, respectively. The curves in those figures represent the behavior at three different concentrations, two below and one in proximity of the critical precipitation concentration, $\phi_M^*$. In general, $p$ decreases with $N_B$. However, the change is more pronounced at a concentration which is close to or slightly above $\phi_M^*$. The inset in Figure 8 shows that $n$ appears to decrease as $N_B$ increases at concentrations below $\phi_M^*$. At $\phi = 0.084$, which is close to or above $\phi_M^*$, the variations in $n$ with $N_B$ are more complicated, depending on when precipitation sets in. At this

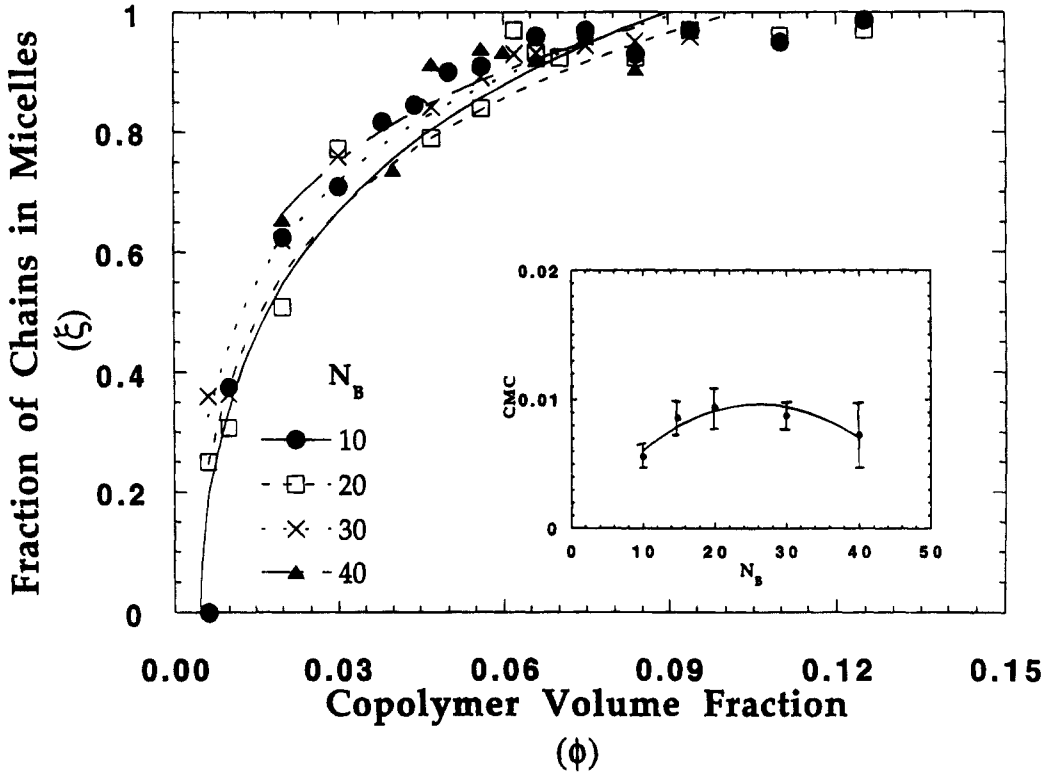


**Figure 7.** Dependence of $\xi$ on $\phi$ for different $N_B$ with $N_A$ constant at 15 and $\beta\epsilon$ at 1. The inset shows the dependence of the CMC on $N_B$.

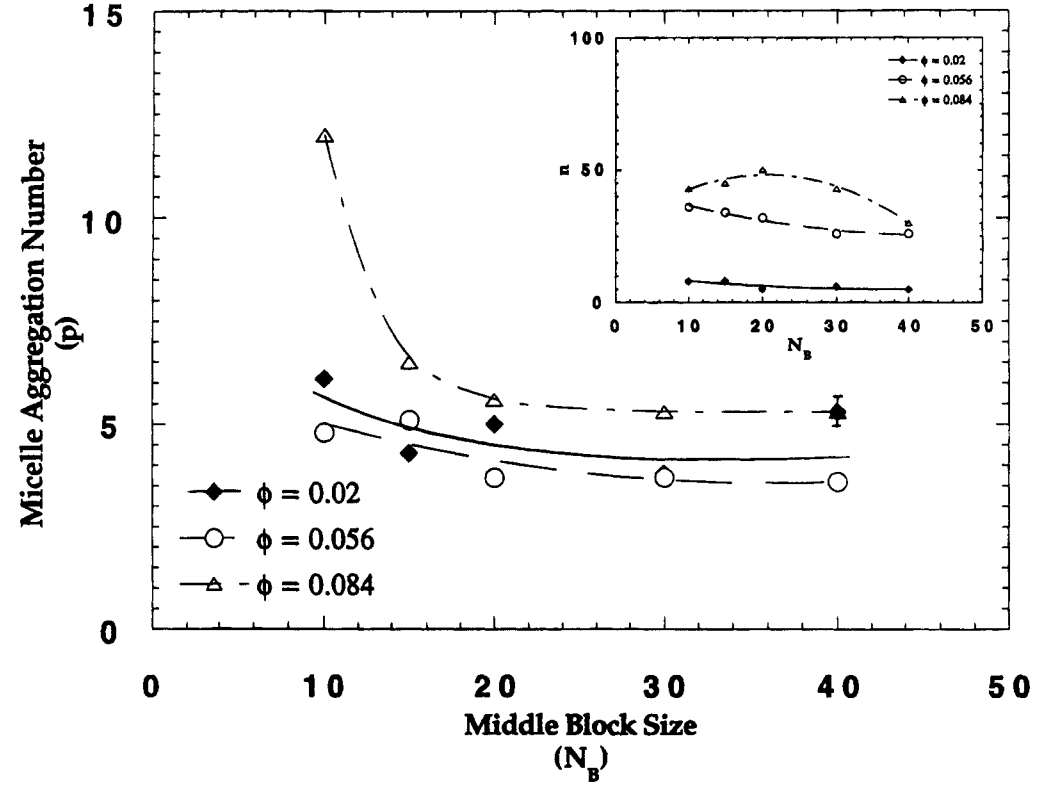


**Figure 8.** Dependence of $p$ and (inset) $n$ on $N_B$ at $\phi = 0.02$ (♦, solid curve), 0.056 (○, dashed curve), and 0.084 (△, dashed/dotted curve).

concentration, $n$ increases and then decreases as $N_B$ increases. Our data suggest that $\phi_M^*$ varies with $N_B$. The actual trend is not predicted due to insufficient data (for $N_B = 15$ and 40). The increase in $N_B$ results in two opposing trends. As $N_B$ increases, the entropic penalty from back-folding of the middle block increases, thus becoming unfavorable for the triblock copolymer chains to form loops. On the other hand, as $N_B$ increases, it becomes increasingly more favorable for the free copolymer chains to form dangling chains at low concentration, and later to convert to bridging chains once enthalpic interactions become significant at high concentration. These entropic effects play significant roles in determining $n$ and $p$.

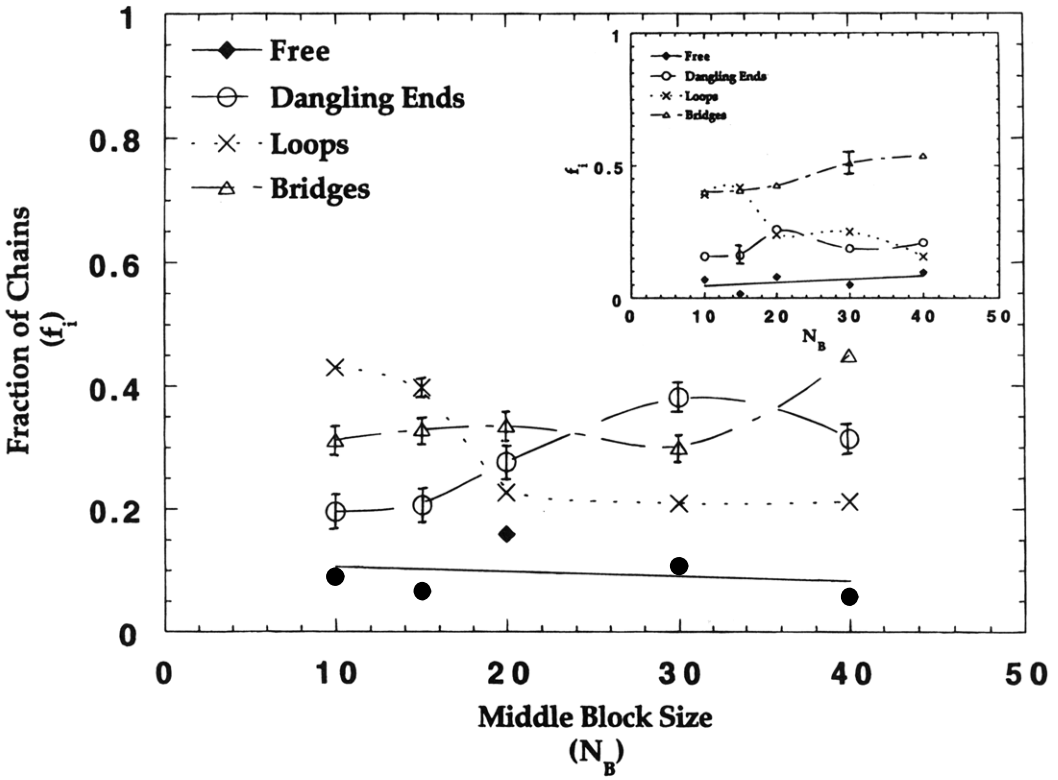


**Figure 9.** Dependence of fraction of (♦, solid curve) free chains, (○, dashed curve) dangling ends, (×, dotted curve) loops, and (△, dashed/dotted curve) bridges with $N_B$ at $\phi$ of 0.056 and (inset) 0.084.

**Chain Population Density.** Figure 9 and its inset show the variations in the chain population distribution at concentrations of 0.056 and 0.084, respectively. These figures show that $f_f$ is relatively insensitive to $N_B$. As expected, the loop fraction, $f_l$, decreases whereas the dangling fraction, $f_d$, increases as $N_B$ increases (due to a corresponding increase in the entropy loss from the back-folding of the middle block) at $\phi = 0.056$. However, the increase in $f_d$ with $N_B$ is less significant at higher concentration due to a conversion of dangling chains to bridges (Figure 9 versus the inset of this Figure). Furthermore, the decrease in $f_l$ is fairly abrupt, resembling a unit step function. On the other hand, we see that the bridging fraction is relatively constant at low $N_B$ and then increases at high $N_B$, being more significant at higher concentrations. Consequently, $N_B$ does not affect the overall micellization process significantly.

**II. Gelation.** Computationally, the system is defined as a gel when there is a group of *interconnecting (or bridging) micelles*, termed a cluster, having bridging chains passing through the box boundaries in all three directions, $x$, $y$, and $z$. With periodic boundary conditions in all three directions, these bridging chains produce an infinitely large three-dimensional network. The two-dimensional representation of the situation that we are specifically interested in is illustrated in Figure 10.

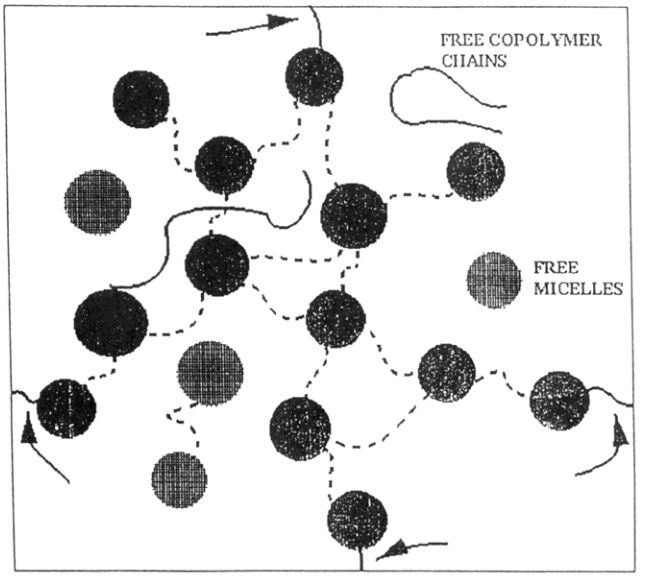


**Figure 10.** Two-dimensional schematic diagram of a network formed from self-association of triblock copolymer chains in selective solvents. The filled and perforated circles represent the networked and free micelles, respectively. For clarity, only the bridging chains are shown as dashed lines. Loops and dangling ends are not shown. The arrows indicate the bridging chains that connect the parent box to the adjacent boxes.

At low concentrations, we see from previous figures that the number of micelles is few and the intermicellar distance is large. Correspondingly, the clusters are relatively small at the low-concentration range. At high concentrations, in comparison, there are more micelles leading to larger clusters. In fact for an infinitely large system, a sol → gel transition point is specified as that concentration at which the cluster molecular weight diverges.[49] In Figure 11a we look at the average cluster size[50] as a function of $\phi$. There is a critical point where the slope of the curve changes discontinuously to a larger value. This polymer concentration is where clusters of micelles begin to attach each other into a larger network. Since the system in the simulation box is of finite size, the cluster molecular weight does not diverge, making it more difficult for determining the transition point exactly using this criteria. However, the point of discontinuity provides a rough estimate of the gel point. Since this method is based on the molecular weight of the cluster, we expect this approach

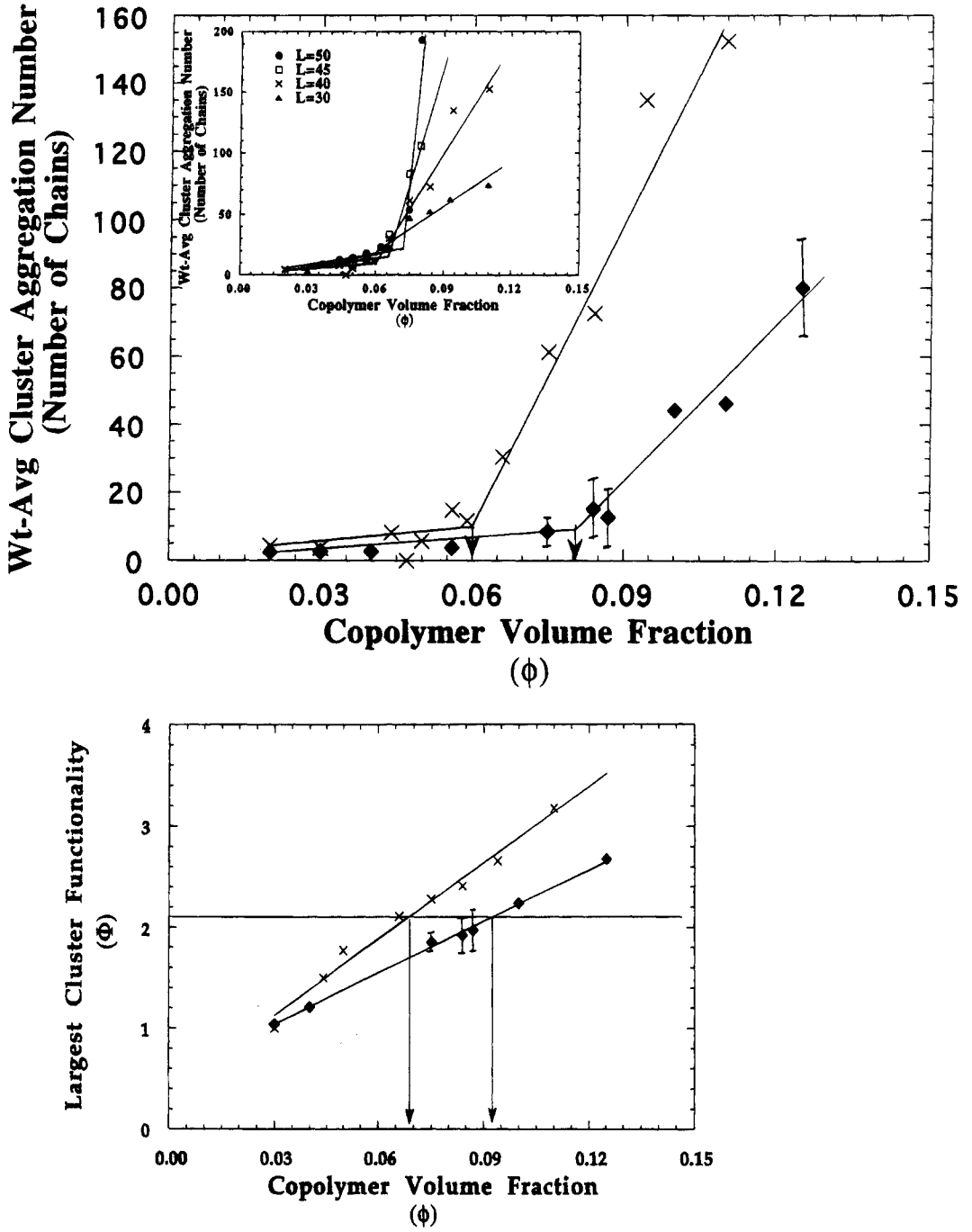


**Figure 11.** Prediction of the gel point using (a, top) cluster molecular weight and (b, bottom) functionality as the criterion illustrated for a system of triblock copolymer chains of $N_A = 15$ and $N_B = 10$ with $2\beta\epsilon N_A$ of (♦) 3 and (×) 30. The inset of Figure 11a shows the average cluster molecular weight as a function of $\phi$ for different $L$ with $N_A = 15$, $N_B = 10$, and $2\beta\epsilon N_A = 30$.

to underestimate the gel point similar to the chemical networks. We denote the critical point thus identified as $\phi_{gel,MW}^*$. As the simulated system becomes larger, the increase in slope would be larger as well (since more clusters will start attaching to the network) and in the limit of $L \rightarrow \infty$ one would observe a divergence at the gel point. The slope of the curve increases as $L$ increases, as illustrated in the inset of Figure 11a, where the average cluster size is shown as a function of $\phi$ for a different box size. The Figure 11a inset also shows that $\phi_{gel,MW}^*$ does not vary much with $L$, when $L$ is changed from 30 to 50. Therefore, our box size is sufficiently large not to affect gelation significantly.

One could also define the sol → gel transition point, $\phi_{gel}^*$, for a system of finite size, using another criterion based upon an analogy with polymerization of multifunctional monomers. Relevant to this criterion are the following network parameters: the number of elastically effective chains, or bridges, $N_e$, and micelle number density, $n_c$, in the largest cluster or the network as it may be. When there are enough bridges, connecting a sufficient number of micelles to span the entire system, gelation occurs. At this critical concentration, the newly formed network coexists with the free micelles and free copolymer chains. The variable which relates $n_c$ and $N_e$ is the functionality, $\Phi$. The largest cluster functionality is defined as the ratio of the total number of bridging chains to the total number of micelles belonging to the cluster (the factor 2 appears since one bridge connects two micelles)

$$\Phi = \frac{2N_e}{n_c} \tag{6}$$

For an infinitely large system of micelles the minimum functionality is 2 for gelation; each micelle must be connected to at least two other micelles. For systems of finite size as in ours, the critical minimum functionality, $\Phi_c^*$, is slightly larger than 2 and corresponds to that of a linear network. For a cluster containing $s$ number of micelles we define $\Phi_c^*$ as

$$\Phi_c^* = \frac{2(s-1)+6}{s} \tag{7}$$

In the limit of infinite $s$, eq 7 gives $\Phi_c^* = 2$. Under the conditions studied in this work, $s$ is a finite number which can be no larger than $M/2$ and $\Phi_c^*$ is typically 2.1.

Figure 11b illustrates how $\phi_{gel}^*$ is determined using $\Phi$ as an indicator. We denote the gel point obtained using the functionality as the criterion as $\phi_{gel,\Phi}^*$. The predicted $\phi_{gel,\Phi}^*$ always turns out to be greater than the $\phi_{gel,MW}^*$ and is believed to be the upper estimate. There are also other methods for predicting the gel point as it pertains to the percolation phenomenon. Namely, the reduced average cluster size,[51] $I'_{avg}$, and the gel fraction[49] (fraction of the copolymer chains in the network), $f_{gel}$, have been used as other criteria for detecting gelation. It has been shown that $I'_{avg}$ exhibits a sharp maximum near the critical percolation point when it is plotted against concentration.[51] Our data also exhibit a sharp maximum in the vicinity of the gel point. Analogous to predicting the CMC, the gel point can also predicted by plotting $f_{gel}$ versus concentration and then extrapolating to zero gel fraction.[49] However, the above two methods require more data in the vicinity of the gel point in order to predict the critical point with the same degree of accuracy as the cluster molecular weight-based and functionality-based methods. Furthermore, the two methods also predict gel points in between the range predicted by the cluster molecular weight and functionality methods. Therefore, in our study we use only the cluster molecular weight and functionality methods.

The most important criterion for gelation for our system of finite size is the geometric condition. This condition requires that in order for the cluster to be considered a three-dimensional network it must be connected to other boxes in all three directions, $x$, $y$, and $z$. In other words, this cluster must have bridging chains passing through the box boundaries in all three directions. It turns out that the copolymer system at $\phi \sim \phi_{gel,\Phi}^*$ always satisfies the geometric condition whereas it is usually not the case with the similar system at $\phi \sim \phi_{gel,MW}^*$. In fact, the functionality of the "network" at $\phi \sim \phi_{gel,MW}^*$ is typically less than 2, which supports our belief that $\phi_{gel,MW}^*$ underestimates the actual gel point. Nevertheless, as will be shown later, $\phi_{gel,MW}^*$ and $\phi_{gel,\Phi}^*$ have similar qualitative trends, providing a range for the gel point.

A question of interest is what parameters does $\phi_{gel}^*$ depend on. From our previous discussion, we know that $\phi_{gel}^*$ is a function of $N_e$ and $n_c$. Since the number of bridging chains, $N_e$, is both a function of incompatibility, or temperature and the end block size, $N_A$, and the middle block size, $N_B$, and $n$ is a function of $N_B$ only, $\phi_{gel}^*$ is expected to be a function of $T$, $N_A$, and $N_B$.

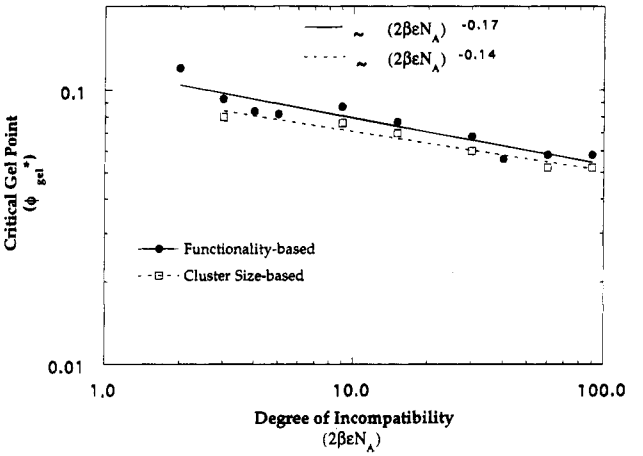


**Figure 12.** Dependence of the functionality-based and molecular weight-based gel point on $2\beta\epsilon N_A$.

$$\phi_{gel}^* = \phi_{gel}^*(T, N_B, N_A) \tag{8}$$

**A. Effects of Incompatibility.** Figure 12 depicts the dependence of both the molecular weight-based and functionality-based critical gel concentration, $\phi_{gel}^*$, on incompatibility, $2N_A\beta\epsilon$. The associated uncertainties are not included since they are smaller than the symbol size. This figure shows that both methods predict qualitatively similar $\phi_{gel}^*$ but the functionality-based $\phi_{gel}^*$ is consistently slightly larger than the molecular weight-based $\phi_{gel}^*$. Figure 12 shows, as expected, that both have a power-law dependence on $2N_A\beta\epsilon$, having approximately the same scaling exponent

$$\phi_{gel}^* \sim x^{-a} \tag{9}$$

where $x$ is a scaling variable $2N_A\beta\epsilon$ and $a$ is in the range 0.1–0.2.

This behavior with $\phi_{gel}^*$ is also reflected in a plot of $N_e$, the number of elastically active or bridging chains in the largest cluster or network as it may be, versus incompatibility, included here as Figure 13. Figure 13 shows that $N_e$ increases as incompatibility increases, coming to a plateau at roughly the incompatibility value of 60. The inset of Figure 13 shows the dependence of functionality $\Phi$ on incompatibility at two concentrations, $\phi = 0.084$ and $\phi = 0.094$. We see here that $\Phi$ changes insignificantly from approximately 2 to less than 3 as $2N_A\beta\epsilon$ increases from 2 to 90, as compared to $N_e$ which changes from ~10 to ~60. Although not included here, the cross-link density $n_c$ (e.g., the number of micelles that are part of the network) increases as incompatibility increases, again leveling off at high incompatibility. These changes have important impacts on the viscoelastic behavior.

The response of a network to a shear strain is completely described by its relaxation modulus. Here, the relaxation modulus, $G_g$, is calculated where $G_g$ in this study is referred to the initial response of a network, $\sigma_0 = G_g\Delta\gamma$, to a small unit step strain $\Delta\gamma$. The analysis of the time-dependent relaxation modulus, although very relevant, is deferred to a subsequent study. The relaxation modulus, $G_g$, is a function of various network parameters, including $N_e$, $\Phi$, and sol; sol is the free micelles and free chains, not attaching to the network. The entanglements of the dangling ends are included as the elastic contribution to the instantaneous response. This is valid for a time scale smaller than the average lifetime of those entanglements. For

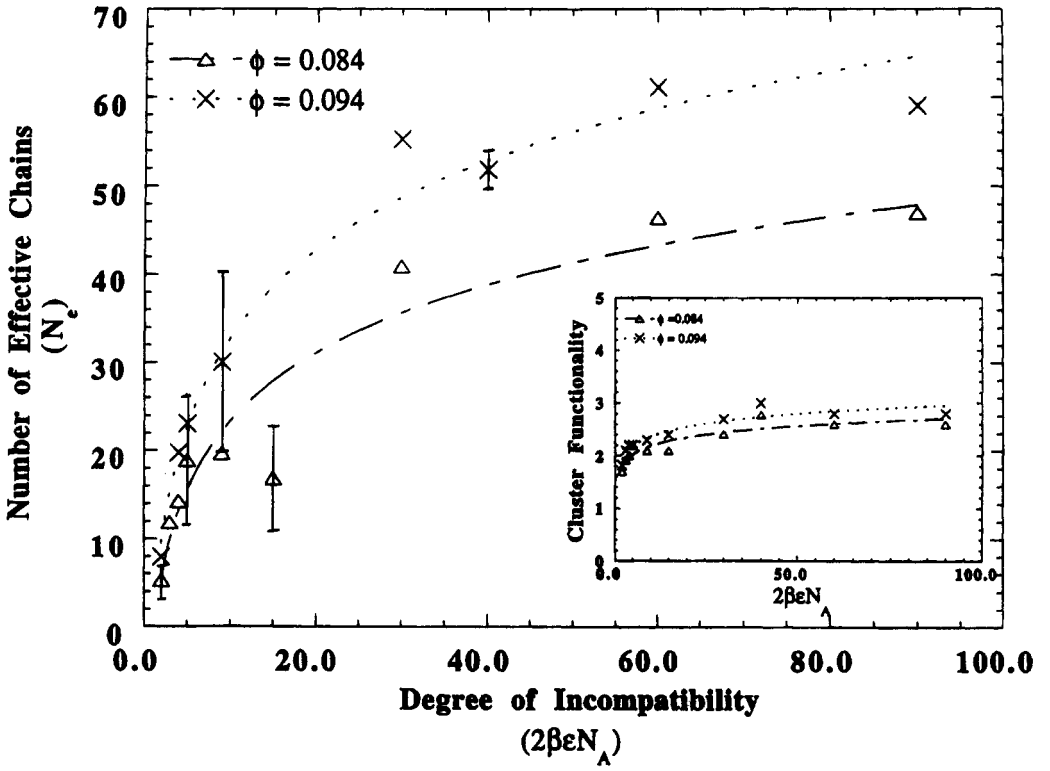


**Figure 13.** Dependence of $N_e$ on $2\beta\epsilon N_A$ at $\phi = 0.084$ (△, dashed/dotted curve) and 0.094 (×, dotted line). The inset shows the dependence of $\Phi$ on $2\beta\epsilon N_A$ at the same concentrations.

a time scale greater than the average lifetime of those entanglements, dangling chains respond to the applied stress only through viscous interactions, contributing insignificantly to the total response. The neglect of the viscous contributions of the free chains and the dangling ends is valid if the average relaxation time of those chains is less than the network lifetime. Loop entanglements, if they occur, would also contribute elastically to the total response. However, for this system which is limited to the dilute regime, loop entanglements have not been observed. Our analysis is valid for systems under low stresses, where the chain number density and the microscopic lifetime of a bridge would not be very much different from those obtained in a quiescent state.

As a first approximation, it is assumed that $G_g$ has a first-order dependence on $N_e$.[52,53]

$$G_g = G_g(N_e, \Phi, \phi_{sol}, \text{etc.}) = G_g(N_e) \qquad (10)$$

or

$$G_g = N_e k_B T \qquad (11)$$

Consequently, Figure 13, which shows the effects of incompatibility on $N_e$, also depicts the dependence of $G_g$, not reflecting the other effects from the micellar properties, including $p$ and micellar compactness. An increase in the micellar aggregation number, $p$, is expected to increase the strength of the junction (by decreasing the extent of fluctuations of the junctions) and thus increase both the modulus and the junction (and bridge) lifetime. Micellar size also has important implications on the network lifetime and elastic modulus. The increase in the compactness of the micelles has the same effects on $G_g$ as $p$ on $G_g$. We have observed that the micelles become more compact in shape as incompatibility increases. We can qualitatively conclude that $G_g$ increases as incompatibility increases,

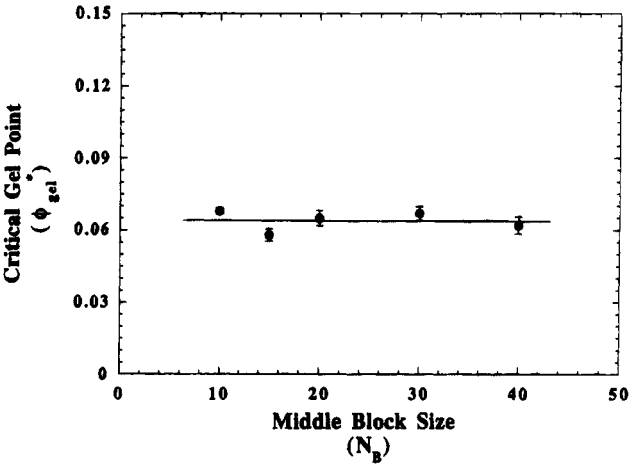


**Figure 14.** Dependence of the critical gel point on $N_B$.

first by an increase in $N_e$ and then subsequently by an increase in both the aggregation number and the compactness of the micelles.

**B. Effects of the Middle Block Size, $N_B$.** The middle block size, $N_B$, affects gelation to a much less significant extent than incompatibility. Figure 14 shows the functionality-based critical gel point, $\phi_{gel}^*$, versus $N_B$. $\phi_{gel}^*$ remains relatively constant as $N_B$ increases from 10 to 40. $N_B$ also has negligible effects on $N_e$. However, we cannot conclude that $N_B$ has no effects on the elastic modulus. The middle block size may influence the network strength by affecting the micellar geometric properties.

## Conclusions

Figure 15 summarizes the effects of the solvent/monomer incompatibility on the association behavior of the triblock copolymer systems, with insoluble end blocks. Our results show conclusively that not only

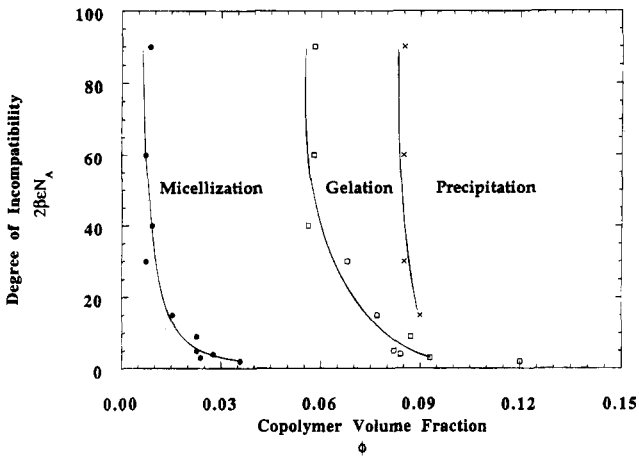


**Figure 15.** Phase diagram of a triblock copolymer system ($N_B$ = 10) with insoluble ends.

micellization but also gelation is possible for this system under certain conditions. This figure also indicates that the phase diagram of this system contains at least four regions. In the first region, below the CMC, the copolymer chains are homogeneously dispersed. In the second region, the micelles along with a few clusters coexist with the free copolymer chains. Above the gel point, enough micelles have bridged to form a gel in the third region. At high concentrations, copolymer systems having intermediate incompatibility levels also exhibit macrophase separation.

Our results show that the association phenomenon is governed by the incompatibility rather than by the soluble block size. Both the critical micelle (CMC) and gel concentrations ($\phi_{gel}$*), decrease as the incompatibility (due to a corresponding increase in the enthalpic contribution) increases, as expected. A scaling behavior is observed for both the CMC and $\phi_{gel}$*, $y \sim x^{-a}$ where $y$ is either the CMC or $\phi_{gel}$*, $x$ is a scaling variable $(2N_A)\beta\epsilon$, and $a$ is approximately 0.4 for the CMC and is in the range 0.1−0.2 for $\phi_{gel}$*. On the other hand, the middle block size $N_B$ has insignificant effects on the above parameters.

**Acknowledgment.** We would like to thank S. Misra for a critical reading of this manuscript. This research was supported by National Science Foundation Grant DMR 9220369.

## References and Notes

(1) Shenoy, A. V. *Colloid Polym. Sci.* **1984**, *262*, 319.
(2) Rehage, H.; Wunderlich, I.; Hoffmann, H. *Prog. Colloid Polym. Sci.* **1986**, *72*, 51.
(3) Ohlendorf, D.; Interthal, W.; Hoffmann, H. *Rheol. Acta* **1986**, 468.
(4) Kramer, O., Ed. *Biological and Synthetic Polymer Networks*; Elsevier Applied Science: New York, 1988.
(5) De Rossi, D.; Kajiwara, K., Osada, Y., Yamauchi, A., Eds. *Polymer Gels: Fundamentals and Biomedical Applications*; Plenum Press: New York, 1991.
(6) Guenet, J.-M. *Thermoreversible Gelation of polymers and biopolymers*; Academic Press: London, 1992.
(7) de Gennes, P.-G. *Solid State Physics*; Academic Press: New York, 1978; Suppl. 14, p 1.
(8) Leibler, L.; Orland, H.; Wheeler, J. C. *J. Chem. Phys.* **1983**, *79*, 3550.
(9) Noolandi, J.; Hong, K. M. *Macromolecules* **1983**, *16*, 1443.
(10) Whitmore, M. D.; Noolandi, J. *Macromolecules* **1985**, *18*, 665.
(11) Zhulina, Ye B.; Birshtein, T. M. *Polym. Sci. USSR* **1985**, *27*, 570.
(12) Munch, M. R.; Gast, A. P. *Macromolecules* **1988**, *21*, 1360.
(13) Nagarajan, R.; Ganesh, K. *J. Chem. Phys.* **1989**, *90*, 5843.
(14) Birshtein, T. M.; Zhulina, E. B. *Polymer* **1989**, *30*, 170.
(15) Kotaka, T.; Tanaka, T.; Inagaki, H. *Polym. J.* **1972**, *3*, 327.
(16) Tanaka, T.; Kotaka, T.; Inagaki, H. *Polym. J.* **1972**, *3*, 338.
(17) Plestil, J.; Baldrian, J. *Makromol. Chem.* **1975**, *176*, 1009.
(18) Tuzar, Z.; Kratochvil, P. *Adv. Colloid Interface Sci.* **1976**, *6*, 201.
(19) Kotaka, T.; Tanaka, T.; Hattori, M.; Inagaki, H. *Macromolecules* **1978**, *11*, 138.
(20) Price, C. In *Development of Block Copolymers*; Goodman, I., Ed.; Applied Science, 1982; Vol I, Chapter 2, p 39.
(21) Balsara, N. P.; Tirrell, M.; Lodge, T. P. *Macromolecules* **1991**, *24*, 1975.
(22) Halperin, A.; Zhulina, E. B. *Europhys. Lett.* **1991**, *16*, 337.
(23) Zhulina, E. B.; Halperin, A. *Macromolecules* **1992**, *25*, 5730.
(24) Halperin, A.; Zhulina, E. B. *Prog. Colloid Polym. Sci.* **1992**, *90*, 156.
(25) Watanabe, H.; Kotaka, T. *Polym. J.* **1982**, *14*, 739.
(26) Hashimoto, T.; Shibayama, M.; Kawai, H.; Wtanabe, H.; Kotaka, T. *Macromolecules* **1983**, *16*, 361.
(27) Watanabe, H.; Kotaka, T. *Macromolecules* **1983**, *16*, 1783.
(28) Leibler, L.; Pincus, P. A. *Macromolecules* **1984**, *17*, 2922.
(29) Tanodekaew, S.; Deng, N.-J.; Smith, S.; Yang, Y.-W.; Attwood, D.; Booth, C. *J. Phys. Chem.* **1993**, *97*, 11847.
(30) Wanka, G.; Hoffmann, H.; Ulbricht, W. *Colloid Polym. Sci.* **1990**, *268*, 101.
(31) Brown, W.; Schillen, K.; Almgren, M.; Hvidt, S.; Bahadur, P. *J. Phys. Chem.* **1991**, *95*, 1850.
(32) Brown, W.; Schillen, K.; Hvidt, S. *J. Phys. Chem.* **1992**, *96*, 6038.
(33) Mortensen, K.; Pedersen, J. S. *Macromolecules* **1993**, *26*, 805.
(34) Malmsten, M.; Lindman, B. *Macromolecules* **1993**, *26*, 1282.
(35) For $N \gg N_e$ where $N$ and $N_e$ are the chain length and the critical entanglement molecular weight, respectively.
(36) Assuming that the chains in the micellar cores are cross-linked or that $T < T_g$, where $T_g$ is the glass transition temperature of the core. The enhanced viscoelastic behavior manifested by the formation of a macrolattice structure disappears upon dilution or an increase in temperature.
(37) A front factor of 2 would be required for symmetric triblock copolymers since there are 2 insoluble end blocks.
(38) Misra, S.; Varanasi, S. *Macromolecules* **1993**, *26*, 4184.
(39) Zhulina, E. B. *Macromolecules* **1993**, *26*, 6273.
(40) Matsen, M. W.; Schick, M. *Macromolecules* **1994**, *27*, 187.
(41) ten Brinke, G.; Hadziioannou, G. *Macromolecules* **1987**, *20*, 486.
(42) Krause, S. *J. Phys. Chem.* **1964**, *68*, 1948.
(43) Tang, W. T.; Hadziioannou, G.; Cotts, P. M.; Smith, B. A.; Frank, C. W. *Polymer Prepr.* **1986**, *27*, 107.
(44) Zhou, Z.; Chu, B. *Macromolecules* **1994**, *27*, 2025.
(45) Linse, P. *Macromolecules* **1993**, *26*, 4437.
(46) Wang, Y.; Mattice, W. L.; Napper, D. *Macromolecules* **1992**, *25*, 4073.
(47) Binder, K. In *Computational Modeling of Polymers*; Bicerano, J., Ed.; Marcel Dekker: New York, 1992.
(48) The factor two appears in front of $f_1$ and $f_b$ but not $f_d$ because loops and bridges contribute two blocks each to the micelles whereas dangling chains contribute only one block each to the micellar cores.
(49) Stauffer, D.; Coniglio, A.; Adam, M. In *Advances in Polymer Science 44*; Dusek, K. Ed.; Springer-Verlag: Berlin, 1982.
(50) If the largest cluster molecular weight, instead of the average cluster molecular weight, is used, a slightly smaller gel point is obtained. The difference is within the experimental uncertainty.
(51) Hoshen, J.; Kopelman, R. *Phys. Rev. B* **1976**, *14*, 3438.
(52) Flory, P. J. *Principles of Polymer Chemistry*; Cornell University Press: Ithaca, NY 1953.
(53) Treloar, L. R. G. *The Physics of Rubber Elasticity*; Clarendon Press: Oxford, U.K., 1975.

MA9413002